

Hybrid connection technologies for hollow sections in steel construction

Circular hollow sections (CHS) offer a variety of constructional and architectural advantages. Up to now, hollow section structures have usually been connected by welding, and more rarely by bolting. However, these established connection methods have disadvantages. Despite its great success in the mobility sector, adhesive bonding is not yet used for joining hollow steel sections in steel construction. Adhesive bonding, however, has significant advantages, especially if combined with classical joining processes. To highlight these advantages, this article presents excerpts from the results obtained in two recently completed research projects. First, a hybrid brace connection for hollow section framework structures is presented which combines welding, bolting and adhesive bonding methods. In addition, the loadbearing behaviour of a novel hybrid grouted connection, which advantageously combines adhesive and grout materials, is analysed and discussed in this paper.

Keywords steel structures; hollow sections; bonded joints; grouted joints; hybrid joints; destructive testing; numerical analysis; K-joint configuration

1 Introduction

Connections for hollow sections in steel construction are currently realized by welding or bolting. Welded circular hollow section joints are used for both longitudinal joints and for connecting braces to continuous chords, e.g. in the joints of lattice structures. Chord joints are mainly provided in the form of full penetration butt-welded connections. Bolted connections for circular hollow sections represent an alternative to welded connections, but they remain marginal in practical applications. In the context of chord joints, bolted flange connections represent an example. However, both connection methods have different disadvantages: With bolted connections, the component cross-section is weakened by holes. With welding, the local energy input during the welding process can lead to disadvantageous effects on shape accuracy, stability and fatigue strength, also static strength in the case of high-strength steels. An overview of the state of the art in the field of hollow section steel structures can be found in [1].

One often underestimated possibility is adhesive bonding as a structural connection method, which offers potential for considerable improvement. This potential can be significantly increased even further by using adhesive bond-

ing technology in hybrid connections. Hybrid connection techniques are already being used successfully in many industrial applications, with adhesive bonding and bolting being frequently combined. In the mobility industry especially, hybrid mechanical/bonded joints are used in a wide range of applications [2]. An overview of hybrid joining techniques is given in [3]. Intensive research is also being carried out in structural steel engineering regarding the combination of bolting and adhesive bonding [4–6]. In the context of this contribution, two recently completed research projects are presented in which adhesive bonding was advantageously combined with classic joining processes. First, an innovative hybrid brace connection for offshore jackets is presented which combines welding, bolting and bonding [7, 8]. After that, a novel hybrid grouted joint is presented in which inorganic grout materials and organic adhesives are used in combination in lap joints for the first time [9].

2 Hollow section framework structures with adhesively bonded bracing

2.1 Foundations for offshore wind turbines

Various types of foundation exist for offshore wind turbines. For water depths of more than 40 m, jacket framework structures consisting of circular hollow sections (CHS) (Fig. 1) represent an alternative to the commonly used monopiles, especially due to their reduced material consumption [10–12]. A disadvantage of the jacket structure is the time-consuming and costly assembly of the loadbearing structure due to the complex joint configurations [13, 14]. The duration of the welding determines the total assembly time. Owing to the spatial intersection of the tubular sections at the framework joints, complex weld seam geometries are usually present. This greatly limits the possibility for using automated welding techniques. An additional complication is the fact that some of the welds must be executed in constrained positions. For final assembly, large open areas are required, as the individual components must be joined in both horizontal and vertical positions (Fig. 1) [15]. Current research focuses on the fatigue behaviour of automated welded joints for offshore structures [16–18].

An alternative node design using cast steel components for jacket structures allows much simpler ring-shaped, semi-automated welding as well as the application of automated processes for the pre-assembly of individual com-

This is an open access article under the terms of the Creative Commons Attribution-NonCommercial-NoDerivs License, which permits use and distribution in any medium, provided the original work is properly cited, the use is non-commercial and no modifications or adaptations are made.

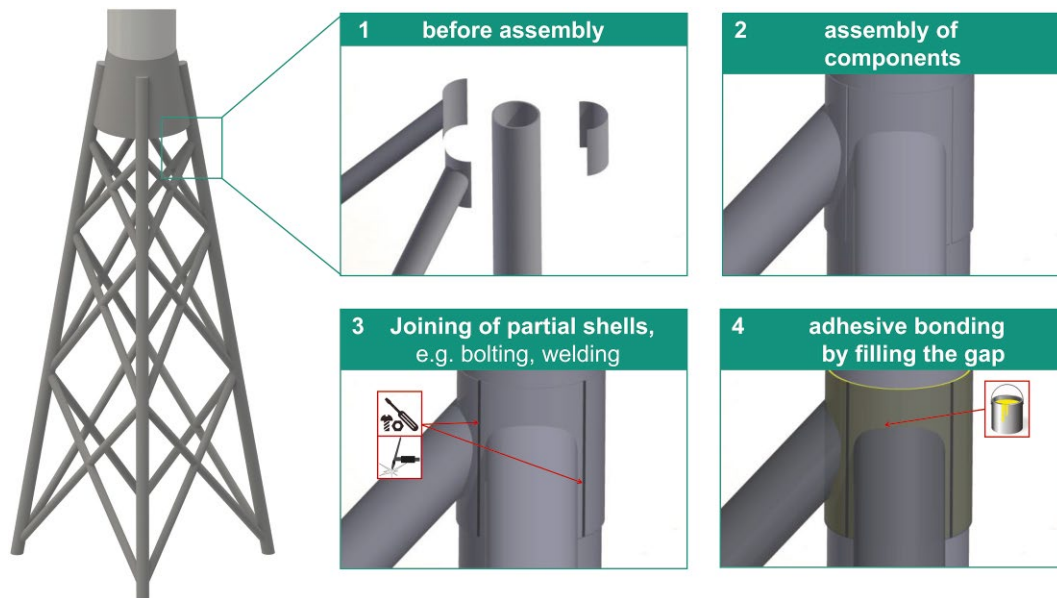


Fig. 1 Concept for hollow section framework with adhesively bonded bracing [23]

ponents [19]. However, the possibilities for using modularized welded structures and parallel production are also severely limited here. In addition, the manual welding work required in the final production step remains high, as the problem of varying assembly positions of the entire jacket structure remains [1, 20]. Thus, there is a considerable need for research to reduce fabrication costs by optimizing the assembly and connection processes. Initial improvements can be achieved by applying adhesive bonding techniques. An adhesively bonded solution for connecting circular hollow sections to cast steel nodes was developed and systematically investigated in [21, 22]. Based on these results, a new type of construction concept was developed in a FOSTA research project [23] which allows considerable further optimization of the production and assembly of steel framework structures by using adhesive techniques in combination with welding and bolting. This concept is the basis for the investigations described in this section and is shown schematically in Fig. 1.

In this construction method, nodal shell segments are welded to the ends of the diagonal bracing components (step 1). These partial shells are designed such that they enclose a circumferential area of up to 180° on the leg component. Assembling the shells produces a complete tubular sleeve (step 2). This means that the leg can initially be easily placed in the open shell segment and does not have to be slid in. In the next step, the shell segments are joined to each other (step 3). This can be carried out by welding the individual partial shells with longitudinal seams or by bolting the end flanges. However, in this step there is no connection between the tubular sleeve and the leg component, i. e. the partial shells form a ring around it. The remaining gap between the tubular sleeve and the wall of the leg component is then joined by adhesive bonding (step 4). This step takes place in the fabrication plant and thus under defined conditions. This construction method has several essential advantages. First of all,

in terms of production technology, modularization is possible because the side parts of the jackets can be prefabricated. This advantage must be compared with the fact that different fabrication steps have to be carried out compared with a welded connection. In addition, the lack of welded connections in the legs results in a significant improvement to the relevant FAT class that has to be considered for fatigue loading. With regard to the material-specific loading conditions of the adhesive layer, this design has the advantage that permanent loads (such as dead weight) are almost completely transferred by the continuous leg components. Thus, dead loads do not cause creep stresses in the adhesive joint. However, adhesive bonding technology has so far hardly been used in steel construction and needs specific design and fabrication skills.

This paper provides an overview of the development and systematic investigation of the hybrid connection concept. Special attention is paid to the numerical calculations carried out at KIT to analyse the stresses in a real jacket as well as the experimental investigations on K-joint test specimens with hybrid joints. All research results are fully detailed in [7–9].

2.2 Representative jacket loadbearing structure and its mechanical stresses

2.2.1 Representative jacket structure

As a basis for the investigations within the scope of this research project, a manufacturer of offshore wind turbines provided the geometry of a representative jacket structure as well as load parameters. The jacket structure consists of four legs and has a height of approx. 50 m. The planned water depth is 30 m and the lower edge of the transition piece is +20 m above normal mean water level. The edge length is 30 m at the base of the jacket and 15 m

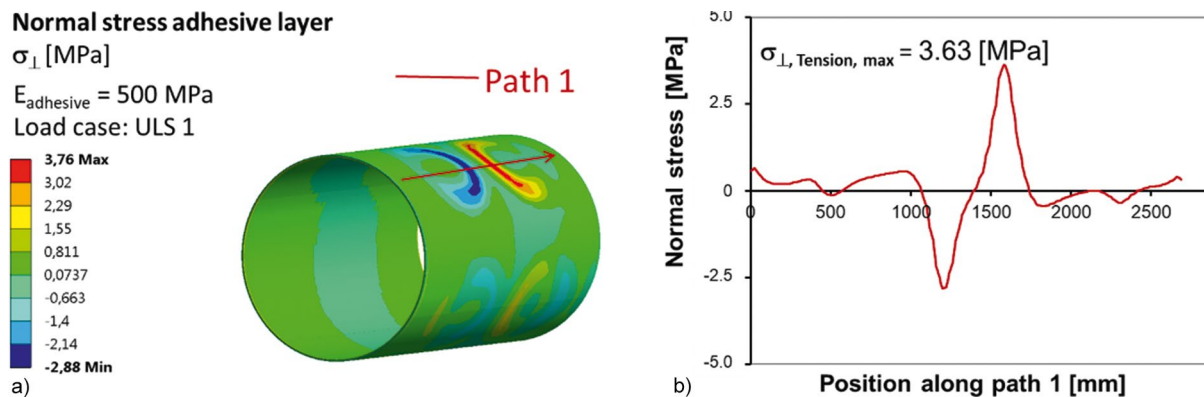


Fig. 2 Typical normal stress distribution in the adhesive layer (normal to adhesive surface) of the bonded jacket structure (a) and evaluation along path 1 (b) [23]

at the top. A total of three diagonal braces (known as bays) are planned. According to the specification of the wind turbine manufacturer, circular hollow sections with a cross-section $D/T = 1422/50 \text{ mm}$ are used for the legs of the jacket structure. The braces consist of circular hollow sections with a cross-section $D/T = 600/40 \text{ mm}$. The dimensions are shown in Fig. 3. There is a reinforced concrete transition piece at the upper end of the steel jacket structure which connects the jacket structure to the tubular steel tower of the wind turbine. The jacket structure is founded on the seabed using suction buckets.

In contrast to the welded jacket structure described above, an alternative node connection as described in section 1 was developed within the scope of this research project [23]. The dimensions of the tubular sleeve are determined in accordance with the dimensions of the increased wall thickness in the joint areas of jacket structures. According to Norsok standard N-004 [24], an increase in the wall thickness of the joint is specified at a distance of $D/4$ or at least 300 mm from the brace connection point. For this purpose, both the corner leg and the braces are initially located on the system lines. The resulting length of the tubular sleeve is extended by the length of the wall thickening required by Norsok standard N-004 [24]. For the relevant joint, the length of the tubular sleeve is 2870 mm. In accordance with the node thickening, the wall thickness of the joint is chosen to be 40 mm. This results in a joint diameter of 1532 mm for an initial typical adhesive joint thickness of 15 mm.

2.2.2 Numerical analysis of mechanical loads

The first question is: How is the loadbearing and deformation behaviour of the whole jacket influenced by the adhesive joints? To analyse this and determine the stresses in the bonded jacket structure, numerical models were generated combining a global framework model with local volume models for the joint areas. The combined numerical model allows both the determination of local stresses in the bonded joint and steel components and the calculation of the global loadbearing behaviour of the jacket with adhesively bonded joints. The individual volume models are connected by beam elements. The founda-

tion of the supporting structure on the seabed is modelled by a fixed support at the base of the legs. The numerical investigations were performed with the ANSYS Workbench software package. Two element types were primarily used for the meshing of the numerical model: The node areas designed as volume models were meshed with the SOLID186 (hexahedron) element type and the areas between the nodes, which are designed as beam models, with BEAM189. The adhesive layer was meshed with two elements over the thickness. The steel and adhesive materials used were implemented in the numerical model with isotropic, linear-elastic material properties. The steel components are assumed to have a modulus of elasticity $E = 210,000 \text{ MPa}$ and a Poisson's ratio $\nu = 0.3$. For the adhesive, different elasticity moduli in the range 5–4000 MPa and Poisson's ratios of $\nu = 0.38$ –0.47 were investigated (Tab. 1).

The dead loads of the transition piece and the wind turbine applied at the top of the real jacket support structure were modelled using individual loads at the top edge of the jacket. In addition, the loading of the wind turbine resulting from wind and turbine operation was integrated into the numerical model as horizontal forces and bending and torsional moments concentrated at this point. The determination of the loads of the jacket support structure due to dead loads, plant operation, wind and wave impact as well as the corresponding load combinations and partial safety factors were chosen in coordination with, or according to, the specification of the manufacturer of the offshore wind turbines involved in the project. The loading due to wave impact was calculated using 9th order stream function wave theory and the specification of Germanischer Lloyd and was applied to legs and diagonals in the numerical model [24, 25].

The determination of the stresses in the adhesively bonded joints is an important objective of the numerical analyses.

For this purpose, the normal stresses orthogonal to the bonded joint layer were evaluated as well as the shear stresses in the plane of the bonded joint. In Fig. 2 the normal stress in the adhesive joint is shown for a representative load case. The tensile or compressive normal stress in

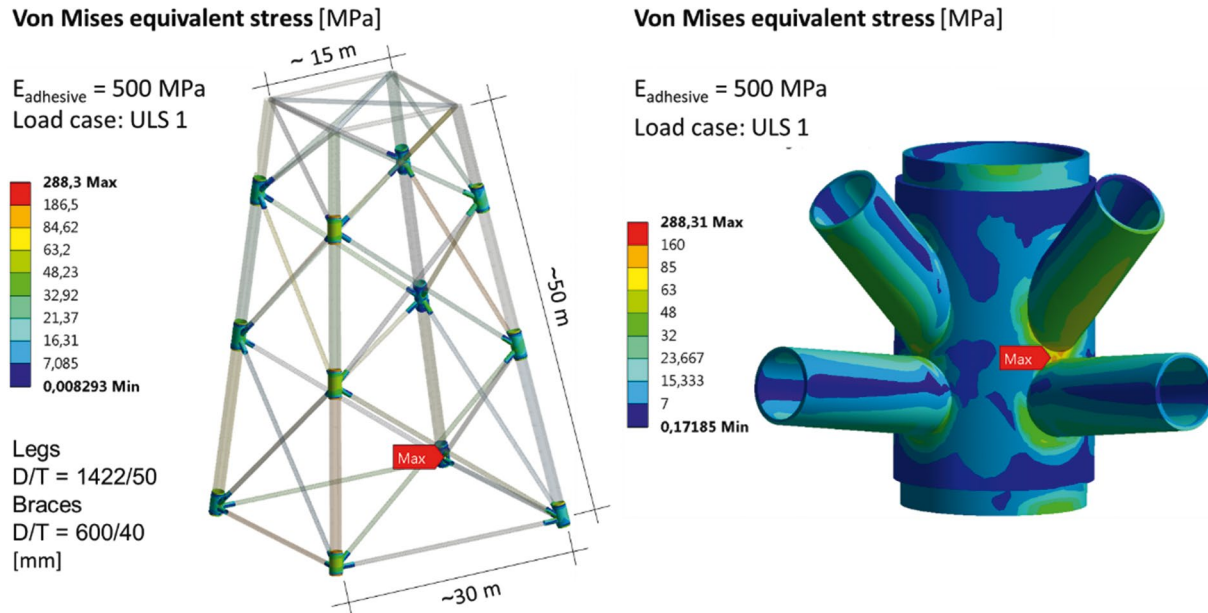


Fig. 3 Von Mises equivalent stresses at the steel nodes [23]

the bonded joint in the areas of the connecting jacket braces can be seen very clearly. For easier illustration of the relevant stress distribution, these are additionally evaluated along a path (Fig. 2a). In keeping with the procedure described, the evaluation of the shear stress is carried out in the plane of the adhesive bonding layer. In addition, the von Mises equivalent stress in the steel structure is evaluated using the volume model for the node with maximum stress. This is shown as an example in Fig. 3. A stress concentration is shown at the weld transition of the connected braces. The analyses are supplemented by the evaluation of the maximum total deformation of the structure.

Extensive numerical calculations were performed to obtain a deeper understanding of the loadbearing behaviour of the hybrid bonded jacket structure. In this context, different geometric and material parameters were varied. The influence of the adhesive stiffness is discussed in this paper by using the investigated adhesive parameters summarized in Tab. 1.

To analyse the influence of the adhesive stiffness acc. to Tab. 1, the maximum normal stress in the adhesive layer evaluated acc. to the procedure described above is plotted over the adhesive stiffness in Fig. 4a. The local stress in the bonded joint increases with increasing stiffness. This can be explained by the increased stiffness of the bonded cross-section, which leads to a higher local stress. A comparable correlation can also be found in Fig. 4b for the

evaluation of the shear stress in the bonded joint as a function of the adhesive stiffness. As the adhesive stiffness decreases, so the associated local adhesive joint stress also decreases. The analysis of the deformation behaviour of the global jacket structure as a function of the adhesive stiffness is especially interesting. For the five selected adhesive stiffnesses, it is shown that there is only a very small variation in the maximum global deformation of the jacket due to different adhesive stiffnesses (Fig. 4d). The quantitative differences are in the order of magnitude of only a few millimetres.

These small differences in the total deformations can be explained by the analysis of the local stresses in the steel structure in the area of the brace connections. In Fig. 4c the Von Mises equivalent stress in the steel joint is shown as a function of the adhesive stiffness. It can be seen that as the stiffness decreases, so there is a redistribution of the stress to the tubular sleeve. This leads to higher local stress concentrations at the welded brace connection. An explanation for this load redistribution could be the softer composite cross-section, consisting of the two steel tubes and the adhesive layer in between, due to the less stiff adhesive.

However, these investigations clearly show that adhesives with very different stiffnesses can be used successfully for the hybrid brace connection. However, it is important to investigate and limit the local stresses in the steel cross-sections.

Tab. 1 Adhesive stiffnesses and Poisson’s ratios investigated

	Adhesive 1	Adhesive 2	Adhesive 3	Adhesive 4	Adhesive 5
Modulus of elasticity	5 MPa	50 MPa	500 MPa	2500 MPa	4000 MPa
Poisson’s ratio	0.47	0.45	0.42	0.38	0.38

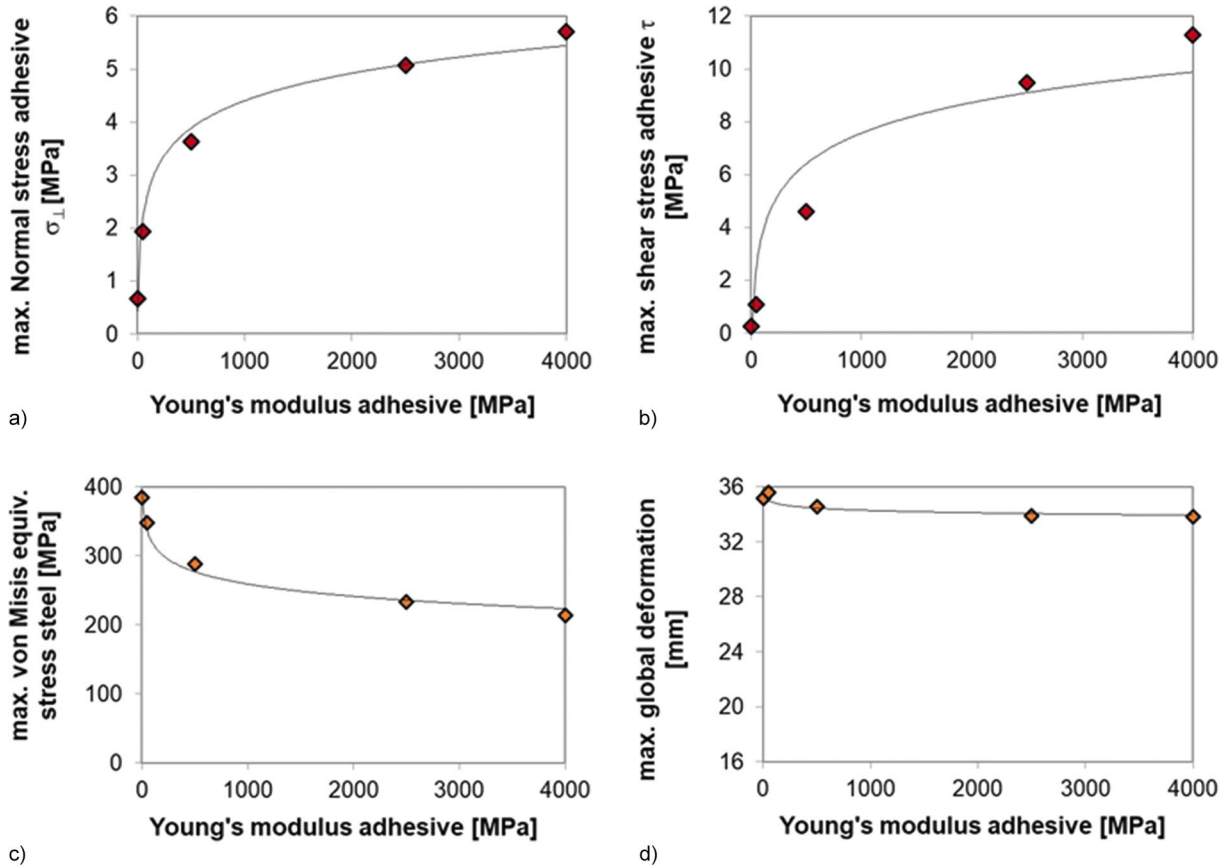


Fig. 4 Numerically calculated stresses in adhesive layer or steel components (a, b, c) and global deformation as a function of the adhesive stiffness (d) [23]

2.3 Adhesive selection and characterization

The preceding sections show that two different adhesive types can be considered for adhesive bonding: Either a stiff, but high-resistance, adhesive, or a less stiff adhesive that does not necessarily exhibit high mechanical strength. Based on a list of requirements and a preliminary investigation of six adhesives, two products were selected and comprehensively characterized for further investigations. Tab. 2 provides an overview of the essential (thermo-)mechanical properties of the two adhesives chosen. It can be seen that based on the results of the numerical investigations, both a highly stiff, structural adhesive (Körapur 4W LV) and an elastic adhesive with significantly lower stiffness (Sika F51) were selected. More detailed information on the adhesives can be found in [8, 23].

2.4 Static tests on adhesively bonded K-joint configurations

The experimental representation of the stress state present in real structures is crucial for the analysis of the

loadbearing behaviour of jacket structures with bonded brace connections. For this reason, tests were carried out on adhesively bonded joints (K-joints). The test specimen designed for the experimental investigations of adhesively bonded K-joints is shown in Fig. 5. The dimensions of the braces, legs and tubular sleeves of the real jacket on which this research project is based were chosen to be scaled by a factor of about 10. All the hollow steel sections of the K-joint are made from S355 steel.

During the adhesive bonding process, a defined surface preparation in the overlap area is the first step. For this purpose, the surfaces of the components to be joined are cleaned with methyl ethyl ketone. In the second step, the surfaces are blasted to quality Sa 3 acc. to DIN EN ISO 8501-1 [26] and then cleaned with methyl ethyl ketone again. At the ends of the intended overlap area, a porous foam tape is applied to the steel tube. The tape prevents lateral leakage of the adhesive, but its porosity allows enclosed air to escape laterally. In the next step, the tubular sleeve with the previously welded braces is pushed onto the leg pipe and centrally aligned. Finally, the adhesive is applied by injecting it into the adhesive

Tab. 2 Selected mechanical parameters of the adhesives selected

	Young's modulus [MPa]	Tensile strength, bulk [MPa]	Shear strength [MPa]	Glass transition temperature [°C]
Körapur 4W-LV	3900 ± 30	47.2 ± 0.6	18.1 ± 2.1	67.1
Sika F51	83 ± 1	4.8 ± 0.1	10.3 ± 3.0	54.8

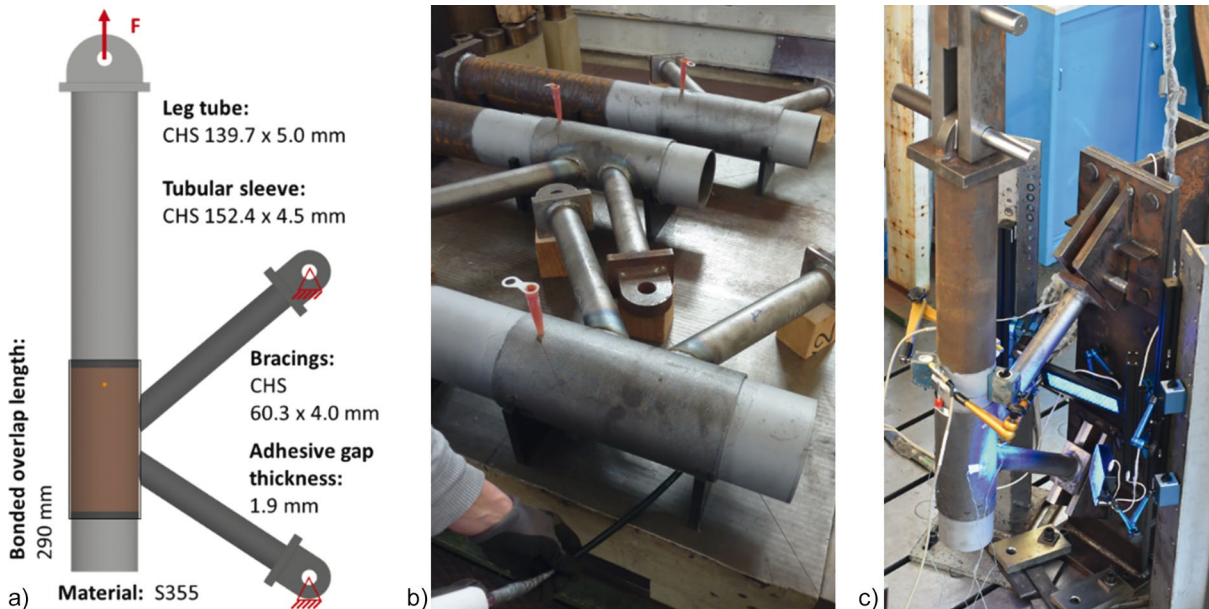


Fig. 5 K-joint test specimen (a), adhesive bonding of K-joints (b) and test setup for quasi-static tests on K-joints (c) [23]

gap. Afterwards, the adhesive production samples are cured at room temperature for at least 21 days.

The test setup used for the experimental investigation of the adhesively bonded K-joints is shown in Fig. 5. The test specimens are fastened to a test setup consisting of a beam in bending fixed to a clamping zone. A servo-hydraulic 1000 kN testing machine applies the load to the end plate welded to the end of the CHS leg.

During the design and construction of the test setup, numerical investigations were carried out to analyse the stress state in the bonded joint as well as in the steel components of the test specimen. In keeping with the procedure described in section 2.2.2, the normal stresses in the adhesive layer orthogonal to the bonding layer and the shear stresses in the plane of the bonded layer were numerically calculated using the Ansys software package. The results of these analyses were compared with the stress states in the bonded joint of the jacket structure determined in section 2.2.2. For both adhesives it can be shown that in the area of the connection of the braces to the tubular sleeve, the stresses in the bonded joint and steel components are of comparable magnitudes.

All tensile tests were carried out with displacement control at a rate of 0.5 mm/min. Machine force and global deformations were recorded. The relative displacements between the tubular sleeve and the CHS leg were recorded during the test using inductive displacement sensors. The sensors are positioned directly at the transition between tubular sleeve and CHS leg. Owing to the large adhesive surfaces between the tubular sleeve and the CHS leg, it is to be expected that a complete failure due to the leg tube being pulled out of the tubular sleeve will not be observed during the test. For this reason, the local strains in the surface of the steel components around the brace connections were determined during the tensile

tests using additional measuring techniques. An optical 3D measuring system was used for this purpose.

In the context of this paper, the focus is on the comparison and analysis of the loadbearing behaviour depending on both adhesives used. The adhesive stiffness differs significantly (by a factor of 50). For each of the two adhesives, five quasi-static tests were carried out on adhesively bonded K-joint test specimens. To discuss the influence of the adhesive stiffness, one test of both adhesives is selected and compared in Fig. 6. The ultimate load capacity of the steel components is achieved for both adhesives. The specimens fail by reaching the yield point at the welded connection between brace and tubular sleeve.

The analysis of the surface strains in the steel components determined by means of the optical measuring system helps to explain the load-deformation behaviour described. Fig. 7 shows the measured true principal strains in the area of the connection between brace and steel tubular sleeve. The main strain values are given in units of per mill. An elongation of 5% is selected as the upper limit value for the colour scale. It can be seen that with increasing machine load in the area of the tensile brace/tubular sleeve connection, large (plastic) strains appear locally in the weld transition area. When the maximum load is reached, a yield zone in the steel cross-section develops in the entire area around the tension brace connection.

Additionally, the influence of the adhesive is also clearly shown in Fig. 6. The load-machine displacement curve of the test specimen with the Sika F51 adhesive ($E = 80$ MPa) flattens at about 200 kN and the specimen shows a decreasing stiffness. The stiffness of the specimen bonded with the Körapur 4W LV adhesive ($E = 4000$ MPa) decreases at a higher load level, which is already accompanied by local steel plastification in the weld transition

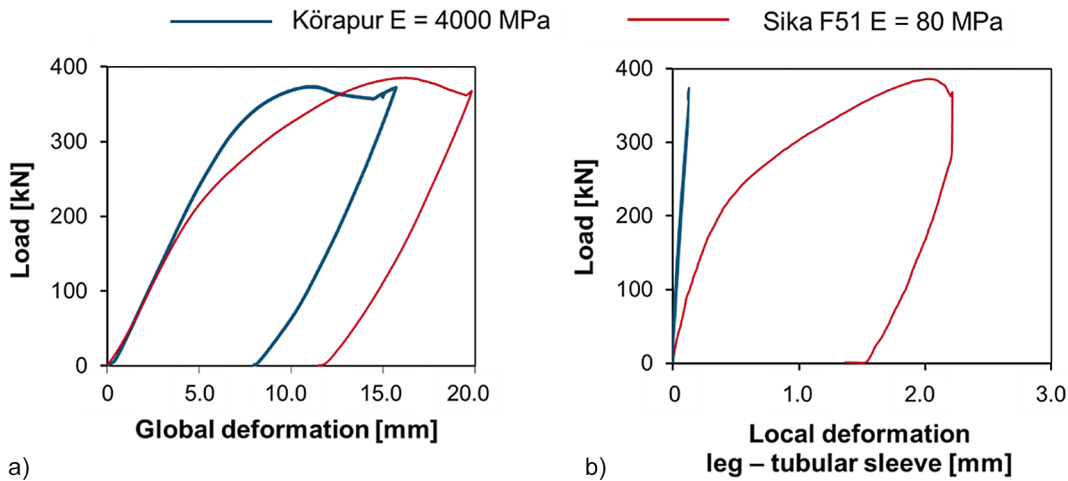


Fig. 6 Comparison of the global (a) and local (b) load-deformation curves for both adhesives [23]

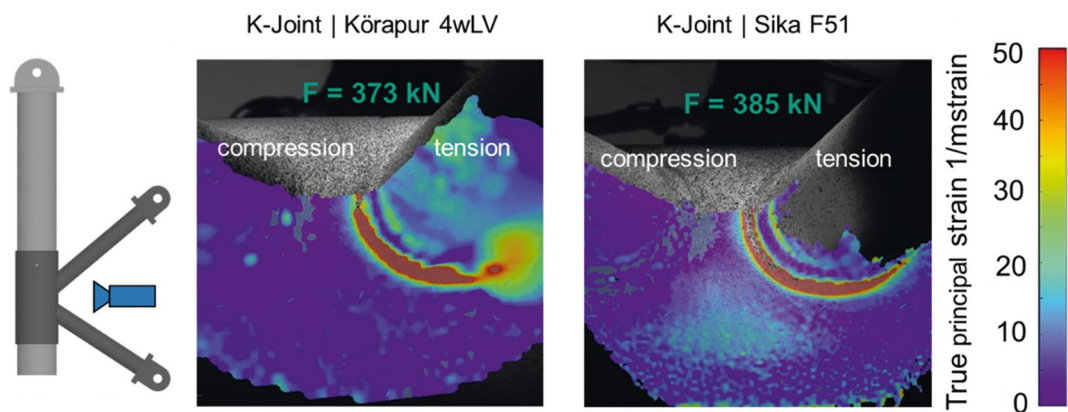


Fig. 7 Component tests on adhesively bonded hollow section K-node; local principal strains in brace connection area [23]

area. The comparison of the two curves also shows that the maximum load capacity is achieved with different machine displacements. The test with the Sika F51 adhesive resulted in an increase in a displacement of about 50%.

A reason for these observations can be derived from the comparison of the local deformations between tubular sleeve and brace hollow section. The machine force is plotted against the local deformations for both tests in Fig. 6. This comparison shows very clearly the influence of the adhesive stiffness. Between tubular sleeve and leg tube, an elastic relative deformation in the range of < 0.2 mm is observed in the specimen bonded with Körapur 4W LV. The influence of the significantly softer Sika F51 adhesive can also be clearly seen in the relative deformation. Fig. 6 shows the bilinear load-deformation curve between the two tubular components. Plastic deformations in the bonded joint are observed, which result in a residual deformation of approx. 1.5 mm after complete unloading.

It should be pointed out here that the loadbearing capacity of the steel components is achieved for both adhesives. This should be particularly emphasized considering the very different stiffnesses of the two adhesives. For example, the Körapur 4W LV adhesive's stiffness ($E = 4000$ MPa) is 50 times higher than that of the

Sika F51 adhesive ($E = 80$ MPa). This difference is also clearly evident in the bond strengths of typical adhesive characterization tests (Tab. 2). However, for the complex, innovative geometry of the K-joint, the ultimate load capacity of the steel components is achieved for both adhesives. This shows the potential of the hybrid connection for joints in CHS framework structures.

2.5 Further investigations of fatigue and ageing loads

The project also involved further investigations of the fatigue and durability of the connection [7, 8, 23]. These can only be briefly addressed in this paper. The tests on the structural behaviour under fatigue loads show that the fatigue strength of the steel structure is critical for failure even under fatigue stress. Any damage that has occurred is initially concentrated around the welded areas between the braces and the tubular sleeve shell. After the end of the test, the failure-relevant areas are examined more closely by cutting the test specimens. Fatigue damage in the area of the bonded joint was not detected. Durability tests reveal the loadbearing behaviour of the bonded joints after ageing. For this purpose, adhesively bonded steel lap shear specimens are exposed to water or salt spray. Tensile tests are carried out after defined ageing periods. Both adhesives exhibit a change in their mechanical properties. The strength degradation for the highly

stiff, structural adhesive is almost linear and reaches a residual strength of approx. 80% after 42 d. In the case of the elastic adhesive, the highest strength degradation takes place in the first 7 d and reduces the strength by approx. 70% compared with the initial strength after 42 d of ageing. For real structures, a permanent sealing of the adhesive joint is therefore necessary. The development of durable sealing is an important task for future research. In the project presented here, which was the first with regard to the new connection technology, the focus was on the mechanical strength of the nodal connection.

3 Hybrid grouted joint for steel structures

3.1 Grouted joint

The grouted joint originated in the offshore oil and gas industry. Today, the grouted joint is frequently used in foundation structures for offshore wind turbines and serves as a structural connection between two circular hollow sections (CHS) of differing sizes. Sliding them into one another results in an overlap. The different diameters lead to an annular gap. This gap is filled on site using a cement-based grout. After curing of the grout material, the connection is able to transfer loads by interlocking. Two design variants must be differentiated: Plain CHS provide minor interlocking potential due to the surface imperfections of the sections. However, welding shear keys on the surface of the opposing surfaces of the CHS significantly improves the performance of the interlocking effect between grout and steel [27].

Both design variants exhibit problems under fatigue loading, especially when used underwater. Plain CHS exhibit a significantly reduced friction between steel and grout due to the presence of water [28]. Additionally, water washes away crushed grout particles. These two mechanisms can lead to critical displacement and, subsequently, failure. Recently, even grouted joints with shear keys exhibited damage at several wind farms [29]. The local stress in the area of the shear keys may exceed the compressive strength of the grout material, which can lead to local failures [30]. Under dry conditions, this has only a minor effect on the service life. However, submerging the grouted joint in water decreases the service life drastically [31]. Relieving the load can lead to water infiltrating into the joint gap. Loading the joint again forces the water out, carrying crushed grout particles with it. This results in cavities that, over time, accumulate and lead to critical relative displacements, which finally lead to joint failure. Hence, for both design variants, the bond properties in the contact area between grout and steel surface are critical for the loadbearing behaviour.

3.2 Construction concept for hybrid grouted joints

The hybrid grouted joint specifically improves this contact area. This connection, developed at the Karlsruhe Insti-

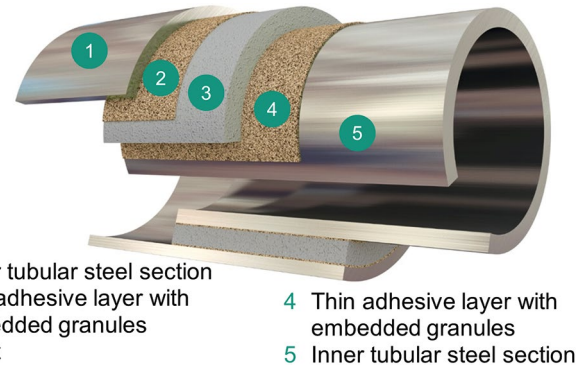


Fig. 8 Hybrid grouted joint [9]

tute of Technology (KIT) by the authors, is characterized by a specific multi-layer composition (Fig. 8). In contrast to state-of-the-art grouted joints, hybrid grouted joints include additional adhesive layers as a substitute for welded shear keys. These layers are applied to the steel surfaces prior to grouting. Sand grains are embedded in these thin adhesive layers before the adhesive has fully cured. After the adhesive has cured, the surface has a high degree of roughness. This creates a high-performance interlock between the grout and the adhesively bonded sand granules extending across the whole contact surface

The combination of grout and adhesive layers has crucial advantages in comparison with welded or bolted joints or conventional organic adhesive bonds and could serve as an alternative to classical joining techniques in structures. First, a high-quality bond and production reliability is achieved by manufacturing the thin-layer adhesive bond under defined and controlled conditions, e. g. in the fabrication plant. Only the grout has to be built in on the construction site; this is a conventional process currently performed in practice. The planned large joint gap allows even large manufacturing and assembly tolerances to be accommodated. Second, the hybrid grouted connection does not introduce any harmful heat into the connected parts and avoids weakening the cross-sections by drilling holes.

The hybrid grouted joint was fully developed in the FOSTA P1307 research project [9]. Extensive analytical, experimental and numerical investigations were carried out to enable the systematic investigation of the hybrid grouted connection. Quasi-static tests determined the axial and bending capacities. Fatigue and durability tests expanded the experimental campaign. Tests on large-scale specimens concluded the project. Owing to the extent of the investigations, only selected experiments and results are presented in this publication. All results are fully detailed in [9, 32, 33].

3.3 Materials

The tubular specimens for the experimental investigations were hot-finished CHS acc. to EN 10025-1 [34] and made of S355J2H. According to the manufacturer's inspection

certificate, the yield strength was $f_y = 404.3$ MPa, the tensile strength $f_u = 552.8$ MPa. The inner CHS had a diameter of 48.3 mm and a thickness of 12.5 mm. The outer section had a diameter of 101.6 mm and a thickness of 10 mm.

“Pagel HF10”, a self-compacting, high-strength grout with good flowability and fast strength development, was used as the grout material. Tests acc. to EN 196-1 [35] determined high values for compressive ($R_c = 123.4 \pm 2.5$ MPa) and flexural ($R_f = 17.9 \pm 1.3$ MPa) strengths after 28 d.

The granules embedded in the adhesive layers were quartz sand with a maximum grain size of 1 mm and very small amount of fine grain (pass ratio for grain size $0.315 \text{ mm} < 1\%$).

The Sikadur-370 adhesive produced by Sika AG was used in the test series presented. It is a two-component epoxy adhesive with high stiffness (modulus of elasticity > 3500 MPa) and high strength (tensile shear strength > 27 MPa). Its high viscosity allows it to be applied to vertical surfaces and overhead.

3.4 Quasi-static axial loadbearing capacity

The quasi-static loadbearing capacity was determined through tests on small-scale hybrid grouted CHS. Overall, 28 different joint compositions with varying materials,

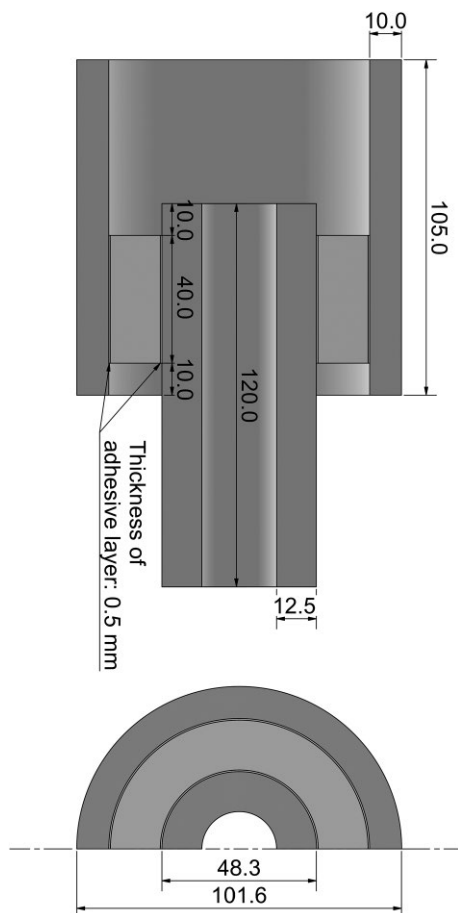


Fig. 9 Specimen geometry for quasi-static experiments [9]

geometry and load directions were tested experimentally. Owing to space limitations, only one test series can be presented as an example in this paper. The test series selected analyses the loadbearing behaviour under compressive load. The length of the hybrid grouted overlap was $L_{ol} = 40$ mm. Fig. 9 shows the specimen geometry.

A servo-hydraulic test rig was used for the experiments. The load was applied directly on the specimen ends using load introduction plates and the tests were conducted with displacement control (test rate: 0.8 mm/min). Calibrated load cells measured the load and two inductive displacement transducers quantified the relative displacement between the two CHS in the area of the overlap. The test was stopped when a critical drop in load occurred.

Fig. 10a shows the experimental setup for the compression tests, and the load-displacement behaviour of the hybrid grouted joints is presented on the right side. All specimens exhibit a very stiff behaviour. Up to 75% of the maximum load, the behaviour can be described as linear-elastic. A reduction in stiffness signals failure, which occurs at an average load $F_{max} = 162.9$ kN. The standard deviation is $SD = 3.5$ kN. This results in a coefficient of variation $c_v = 2.2\%$. The average maximum nominal shear stress as a quotient of maximum load and adhesive area

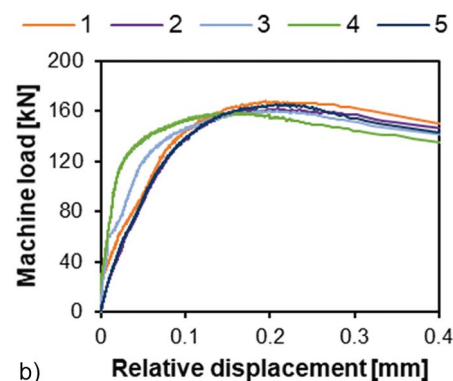


Fig. 10 Experimental setup for quasi-static compressive experiments (a) and load-displacement diagram for the selected series (b) [9]

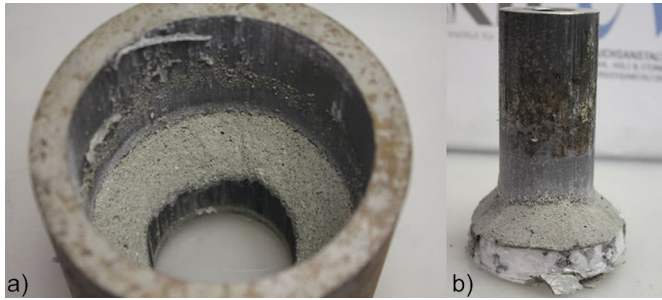


Fig. 11 Fracture patterns of outer (a) and inner (b) sections [9]

on the inner CHS is $\tau_{\max} = 26.8$ MPa. Maximum load occurs at a relative displacement of about 0.2 mm. Examining the fracture patterns (Fig. 11) shows that all specimens failed in a similar way. Near-interface failure in the inner adhesive layer dominates the fracture pattern. Most of the grout layer remains attached to the outer CHS. Some specimen show fracture cones in the grout layer. These cones adhere to the inner CHS.

The hybrid grouted joint exhibits high loadbearing capacities with marginal scatter across all test series with varying gap sizes and overlap lengths as well as different adhesive and grout materials. Based on the analysis of the fracture patterns, adhesive failure on the side of the inner CHS can be observed. Fracture cones in the grout layer seem to form at an early load stage (when the local tensile

strength of the grout is surpassed) and are not significant for the global joint performance. For the geometries investigated, loadbearing capacity and overlap length are related linearly. Based on this, an overlap length of 125 mm would be sufficient to reach the elastic loadbearing capacity of the inner CHS. The results of test series with artificially induced imperfections are of special interest. It was shown that neither canting nor eccentric alignment of the inner CHS reduces the loadbearing capacity. A detailed description of all test series can be found in [9].

3.5 Quasi-static bending capacity

The behaviour of the hybrid grouted joint under pure bending was investigated by performing various test series. The test was conducted as a four-point bending test. The test series presented in detail as an example in this publication has the same cross-section geometries and materials as given in section 2.4. Fig. 12 shows the geometry of the bending specimens. Three hybrid grouted specimens were tested in each series. The length of the hybrid grouted overlap was 78 mm, which corresponds to 1.2 times the medial diameter of the specimen.

The applied displacement rate was 1.0 mm/min. Inductive displacement transducers measured the global deflection in the area of the overlap. Fig. 13a shows the test

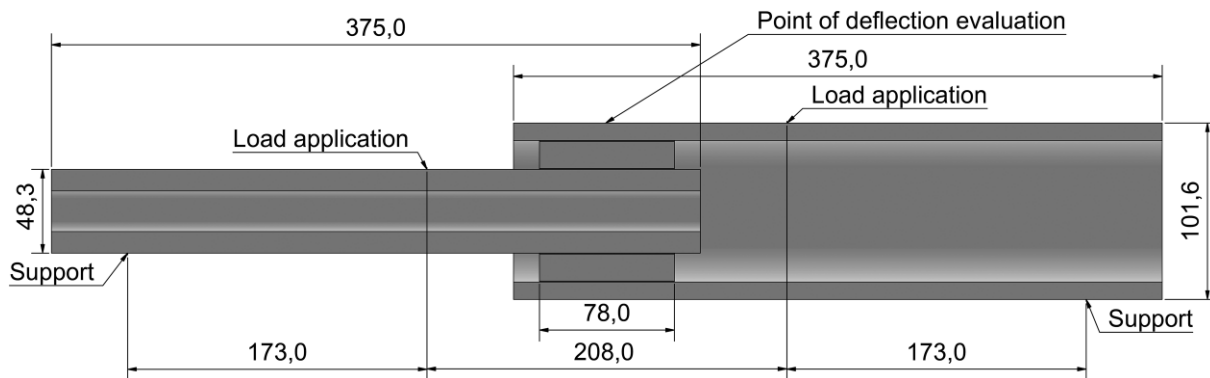


Fig. 12 Geometry of bending specimen [9]

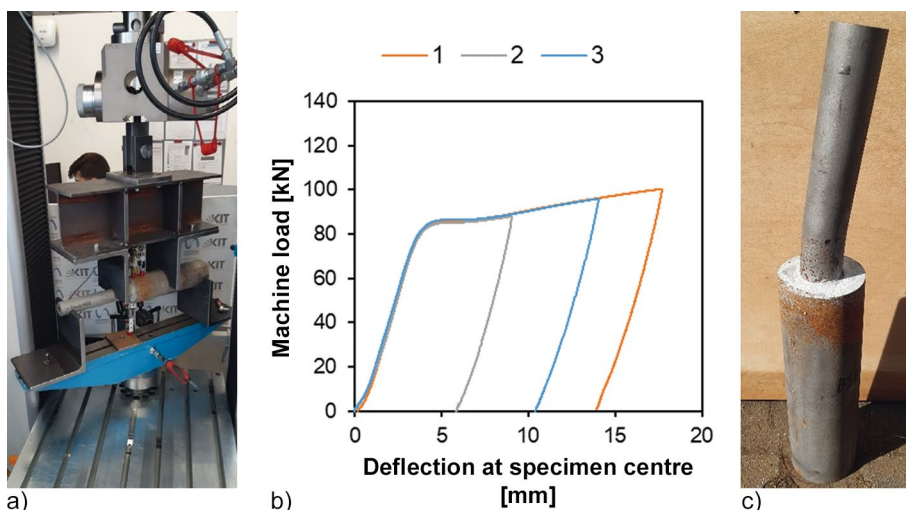


Fig. 13 Test setup for bending specimen (a), load-deflection diagram (b) and deflected specimen (c) [9]

Tab. 3 Fatigue stresses for different stress levels

Maximum static shear strength $\tau_{Adh,u,stat}$ [MPa]	Fatigue stress range $\Delta\tau_{Adh,fat}$ [MPa]	$\Delta\tau_{Adh,fat}/\tau_{Adh,u,stat}$ [-]	Upper load [kN]	Lower load [kN]	Mean load [kN]	Number of specimens tested [-]
	13.6	0.51	91.2	9.12	50.16	3
26.8	15.5	0.58	104.2	10.42	57.31	6
	17.4	0.65	117.2	11.72	64.46	4

setup. Evaluating the deflection at the specimen centre (Fig. 13) shows that all specimens have a similar load-deflection behaviour (Fig. 13b). Increasing deformation led to a linear increase in the load being observed until the plastic bending resistance of the inner cross-section was reached (as the product of plastic section modulus and yield strength). The appearance of a plastic hinge in the inner CHS close to the hybrid setup is accompanied by a significant reduction in the bending stiffness. As deformation increases further, a nearly linear load-deformation behaviour is observed. Inspecting the specimen after the test reveals that there is no visible damage in the hybrid grouted joint. In contrast, the plastic deformation in the steel section is clearly visible (Fig. 13c).

The bending tests show that the hybrid grouted joint has a high bending resistance. All test specimens reached the plastic bending resistance of the smaller CHS being connected.

3.6 Fatigue behaviour

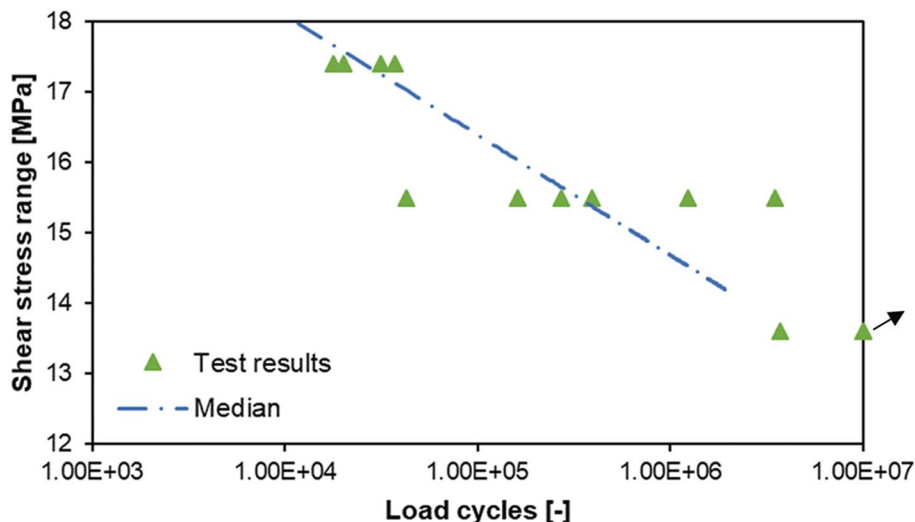
Fatigue tests were conducted on the specimens presented in section 2.4. The main aim was to identify the relation between fatigue life and stress range. Therefore, tests were conducted on three different stress levels. For all fatigue tests, the test frequency was 8 Hz and the fatigue stress ratio 0.1. The respective stress range is defined as a fraction of the quasi-static shear strength.

Tab. 3 shows the fatigue stresses for the different stress levels investigated. It also lists the number of specimens tested at each stress level. On the highest stress level ($\Delta\tau_{Adh,fat} = 17.4 \text{ MPa} \cong 0.65 \tau_{Adh,u,stat}$), the hybrid grouted joints show between 18,000 and 37,305 load cycles. Monitoring the machine displacement at mean load shows that there is virtually no displacement until immediately before failure. The fracture pattern is congruent to the quasi-static test series.

On the middle stress level ($0.58 \tau_{Adh,u,stat}$), the number of cycles until failure scatters considerably. The lowest number is 43,007 cycles, the highest 3,483,327 cycles. The displacement behaviour is similar to the higher stress level, as is the fracture pattern.

On the lower stress level ($0.51 \tau_{Adh,u,stat}$), very high cycle numbers are reached. Two experiments were stopped without failure (runouts), one after 10 mio. load cycles, the other after 19 mio. The third one failed at 3,750,190 load cycles.

Fig. 14 summarizes the results of the fatigue tests. First, it is apparent that the hybrid grouted joint possesses a high resistance against fatigue loads. For a stress level of 50% of the static shear strength, runouts or very high load cycle numbers can be seen. Increasing the stress level reduces the fatigue life. The documented high scatter on the middle stress level is well known in the literature [36]. Here, details are particularly prone to imperfections due to ge-

**Fig. 14** Wöhler diagram of the fatigue tests [9]

ometry, materials or manufacturing. Considering all results, a half-logarithmic relation between stress level and service life can be assumed. However, this relation should be supported by more fatigue tests. Comparing these results with state-of-the-art welded CHS connections shows that the hybrid grouted connection represents a very promising alternative. The best possible fatigue class for comparable welded connections is FAT71. Assuming a fatigue strength of 14 MPa for the hybrid grouted connection results in the fact that, for the geometry presented and an overlap length of only 50 mm, the fatigue resistance of the best possible welded connection is surpassed. The fatigue behaviour of the hybrid grouted joint underwater will be investigated in a follow-up project.

4 Conclusions

The use of adhesive bonding technology for connecting hollow sections has not yet been established. However, research projects completed recently show that adhesive bonding can lead to significant advantages, especially in combination with classic joining processes. To highlight these advantages, extracts from research results are presented in this paper.

Firstly, an innovative connection concept for jacket structures combines adhesive bonding, bolting and welding. The local stresses in the adhesively bonded joint and the steel structure were determined in numerical analyses. It was found that due to the specific design concept, both high-modulus structural adhesives and low-modulus adhesives can be used. However, the stiffness of the adhesive has an influence on the local steel stresses. The structural behaviour of the joint was analysed in experimental investigations of bonded K-joint configurations. The ultimate load capacity of the steel components was always reached for both a stiff and a low-modulus adhesive. Differences resulting from the adhesive used can be seen in the global and local deformations between tubular sleeve and leg component. The results of this research project clearly show the high potential of the hybrid, bonded bracing connection. The innovative design principle opens up new design and construction possibilities for loadbearing structures made of hollow sections.

Secondly, a newly developed hybrid grouted joint is presented which is characterized by a specific multi-layered composition. In contrast to state-of-the-art grouted joints, hybrid grouted joints include additional adhesive layers

as a substitute for welded shear keys. These layers are applied to the steel surfaces prior to grouting. Extensive analytical, experimental and numerical investigations were carried out for the systematic investigation of the hybrid grouted connection. In all test series, the hybrid grouted joint shows a high loadbearing capacity (bond strengths up to 30 MPa). In bending tests carried out during the project, the plastic loadbearing capacity of the tubular cross-sections was achieved without any failure of the joint being detected. The loadbearing and failure behaviour of the hybrid grouted tube connection under fatigue loading was investigated under axial compression stress. The adhesive-grout combinations tested show a high fatigue resistance. According to DIN EN 1993-1-9 [37], fatigue strength is the stress range a construction detail can withstand for more than 5 mio. load cycles. Based on the tests carried out, for the hybrid grouted joint this fatigue strength is approx. 50% of the quasi-static loadbearing capacity. The results of the research project demonstrate the good performance of the new hybrid grouted connection technology. Owing to the high loadbearing capacities determined in this project under quasi-static and non-static loads, the hybrid grouted joint shows high potential for applications in steel construction, especially in combination with cast steel nodes. Using this technique, a connection is possible which is able to transfer the full axial capacity of the CHS connected, even for high-strength steels. This is a clear advantage compared with traditional joint construction and helps to reduce weight and resource needs.

Acknowledgments

The IGF No. 18969 N/FOSTA P 1123 and IGF No. 19989 N/FOSTA P 1307 research projects of the Forschungsvereinigung Stahlanwendung e.V., Sohnstraße 65, 40237 Düsseldorf, were supported by the Federal Ministry of Economics & Energy through the German Federation of Industrial Research Associations (AiF) as part of the programme for promoting industrial cooperative research. We would like to thank our research partners Fraunhofer Institute for Manufacturing Technology and Advanced Materials IFAM (Bremen, Germany) and the Munich University of Applied Science for the good collaboration.

Open access funding enabled and organized by Projekt DEAL.

References

- [1] Wardenier, J. (2010) *Hollow sections in structural applications*. CIDECT. Bouwen met Staal.
- [2] Maggiore, S.; Banea, M. D.; Stagnaro, P.; Luciano, G. (2021) *A Review of Structural Adhesive Joints in Hybrid Joining Processes*. *Polymers* 13, no. 22. <https://doi.org/10.3390/polym13223961>
- [3] Fricke, H.; Vallée, T. (2021) *Hybrid joining techniques*. *Advanced Joining Processes*, pp. 353–381.
- [4] Vallée, T.; Fricke, H.; Myslicki, S.; Kaufmann, M.; Voß, M.; Denkert, C.; Glienke, R.; Dörre, M.; Henkel, M.-K.; Gerke, T. (2021) *Modelling and strength prediction of pre-tensioned hybrid bonded joints for structural steel applica-*

- tions. *The Journal of Adhesion*, pp. 1–41. <https://doi.org/10.1080/00218464.2021.1928498>
- [5] Denkert, C.; Gerke, T.; Glienke, R.; Dörre, M.; Henkel, M. K.; Fricke, H.; Myslicki, S.; Kaufmann, M.; Voß, M.; Vallée, T. (2021) *Experimental investigations on pre-tensioned hybrid joints for structural steel applications*. *The Journal of Adhesion*, pp. 1–36. <https://doi.org/10.1080/00218464.2021.2003786>
 - [6] Boretzki, J.; Albiez, M. (2022) *Static strength and load bearing behaviour of hybrid bonded bolted joints: experimental and numerical investigations*. *Journal of Adhesion*. <https://doi.org/10.1080/00218464.2022.2033619>
 - [7] Albiez, M.; Damm, J.; Ummerhofer, T.; Ehard, H.; Schuler, C.; Kaufmann, M.; Vallée, T.; Myslicki, S. (2021) *Hybrid joining of jacket structures for offshore wind turbines – Validation under static and dynamic loading at medium and large scale*. *Engineering Structures* 252, 113595. <https://doi.org/10.1016/j.engstruct.2021.113595>
 - [8] Albiez, M.; Damm, J.; Ummerhofer, T.; Kaufmann, M.; Vallée, T.; Myslicki, S. (2021) *Hybrid joining of jacket structures for offshore wind turbines – Determination of requirements and adhesive characterisation*. *Engineering Structures* 252, 114186. <https://doi.org/10.1016/j.engstruct.2022.114186>
 - [9] Ummerhofer, T.; Albiez, M.; Boretzki, J. et al. (2021) *Hybride Grout-Verbindungen für Stahlbaukonstruktionen (HybridGrout)*. Forschungsprojekt FOSTA P 1307/IGF-Nr. 19989 N, Final report.
 - [10] Konstantinidis, E. I.; Botsaris, P. N. (2016) *Wind turbines: current status, obstacles, trends and technologies*. IOP Conference Series: Materials Science and Engineering 161, 12079. <https://doi.org/10.1088/1757-899X/161/1/012079>
 - [11] Sánchez, S.; López-Gutiérrez, J.-S.; Negro, V.; Esteban, M. D. (2019) *Foundations in Offshore Wind Farms: Evolution, Characteristics and Range of Use. Analysis of Main Dimensional Parameters in Monopile Foundations*. *Journal of Marine Science and Engineering* 7, no. 12, pp. 441. <https://doi.org/10.3390/jmse7120441>
 - [12] Rusu, E. (2020) *An evaluation of the wind energy dynamics in the Baltic Sea, past and future projections*. *Renewable Energy* 160, pp. 350–362. <https://doi.org/10.1016/j.renene.2020.06.152>
 - [13] Brauser, S.; Michels, G. (2018) *Industrieller Offshore-Wind-Jacketbau durch seriell vorgefertigte Komponenten (Industrial offshore wind jacket construction through serially pre-fabricated components)*. VDI ingenieur forum 60, H. 2.
 - [14] Wu, X.; Hu, Y.; Li, Y.; Yang, J.; Duan, L.; Wang, T.; Adcock, T.; Jiang, Z.; Gao, Z.; Lin, Z.; Borthwick, A.; Liao, S. (2019) *Foundations of offshore wind turbines: A review*. *Renewable and Sustainable Energy Reviews* 104, pp. 379–393. <https://doi.org/10.1016/j.rser.2019.01.012>
 - [15] Michels, G.; Brauser, S. (2014) *Supply Chain Concept for Industrial Assembling of Offshore-Wind-Jackets* in: Conference Proceedings of the International Wind Engineering Conference Hannover. IWEC, Hannover, 2./3. Sept. 2014.
 - [16] Schürmann, K. (2019) *Prediction of the Initial Fatigue Crack Location of Automatically Welded Tubular Joints for Jacket Support Structures* in: 7th International Conference on Structural Engineering, Mechanics and Computation. SEMC, Cape Town, Sept. 2–4, 2019. <https://opus4.kobv.de/opus4-bam/frontdoor/index/index/docId/51872>
 - [17] Schürmann, K.; Schaumann, P.; Pittner, A.; Rethmeier, M. (2020) *Experimental investigations on the fatigue resistance of automatically welded tubular X-joints for jacket support structures*. *Journal of Physics: Conference Series* 1669, no. 1, 12022. <https://doi.org/10.1088/1742-6596/1669/1/012022>
 - [18] Schürmann, K. W. (2021) *Fatigue Behavior of Automatically Welded Tubular Joints for Offshore Wind Energy Substructures* [Dissertation]. Gottfried Wilhelm Leibniz Universität Hannover.
 - [19] Nagel, S.; Spannaus, M.; Ummerhofer, T. (2019) *Stahlguss – ein unterschätzter Werkstoff* in: Kuhlmann, U. [Hrsg.] *Stahlbau Kalender 2019*. Berlin: Ernst & Sohn, S. 433–479.
 - [20] Kanyilmaz, A. (2019) *The problematic nature of steel hollow section joint fabrication, and a remedy using laser cutting technology: A review of research, applications, opportunities*. *Engineering Structures* 183, pp. 1027–1048. <https://doi.org/10.1016/j.engstruct.2018.12.080>
 - [21] Albiez, M.; Vallée, T.; Fricke, H.; Ummerhofer, T. (2019) *Adhesively bonded steel tubes – Part I: Experimental investigations*. *International Journal of Adhesion and Adhesives* 90, pp. 199–210. <https://doi.org/10.1016/j.ijadhadh.2018.02.005>
 - [22] Albiez, M.; Vallée, T.; Ummerhofer, T. (2019) *Adhesively bonded steel tubes – Part II: Numerical modelling and strength prediction*. *International Journal of Adhesion and Adhesives* 90, pp. 211–224. <https://doi.org/10.1016/j.ijadhadh.2018.02.004>
 - [23] Ummerhofer, T.; Albiez, M.; Damm, J. et al. (2019) *Hohlprofilfachwerkstrukturen mit geklebten Strebenanschlüssen – KlebStreb*. Forschungsprojekt FOSTA 1123, IGF Nr. 18969 N.
 - [24] Norsok standard N-004 (2004) *Design of steel structures*.
 - [25] DIN EN 61400-3-1:2019 (2019) *Windenergieanlagen – Teil 3-1: Auslegungsanforderungen für gegründete Offshore-Windenergieanlagen*. Berlin: Beuth.
 - [26] DIN ISO 8501-1:2007 (2007) *Visuelle Beurteilung der Oberflächenreinheit – Teil 1: Rostgrade und Oberflächen-vorbereitungsgrade von unbeschichteten Stahloberflächen und Stahloberflächen nach ganzflächigem Entfernen vorhandener Beschichtungen*. Berlin: Beuth.
 - [27] Billington, C. J.; Lewis, G. H. (1978) *The Strength of Large Diameter Grouted Connections*. Offshore Technology Conference 1978, Paper OTC 3083. Houston, May 1978. <https://onepetro.org/OTCONF/proceedings-abstract/78OTC/All-78OTC/OTC-3083-MS/47314>
 - [28] Dallyn, P.; El-Hamalawi, A.; Palmeri, A.; Knight, R. (2016) *Experimental investigation on the development of wear in grouted connections for offshore wind turbine generators*. *Engineering Structures* 113, pp. 89–102. <https://doi.org/10.1016/j.engstruct.2015.11.028>
 - [29] Schaumann, P.; Lochte-Holtgreven, S.; Lohaus, L.; Lindschulte, N. (2010) *Durchdruchende Grout-Verbindungen in OWEA – Tragverhalten, Instandsetzung und Optimierung*. *Stahlbau* 79, H. 9, S. 637–647. <https://doi.org/10.1002/stab.201001357>
 - [30] Bechtel, A. C. (2016) *Fatigue Behaviour of Axially Loaded Grouted Connections in Jacket Structures* [Dissertation]. Gottfried Wilhelm Leibniz Universität Hannover.
 - [31] Raba, A. (2018) *Fatigue behaviour of submerged axially loaded grouted connections* [Dissertation]. Gottfried Wilhelm Leibniz Universität Hannover.
 - [32] Myslicki, S.; Vallée, T.; Boretzki, J.; Albiez, M.; Ummerhofer, T. (2021) *Hybrid bonded joints combining organic and inorganic adhesives: development and validation of an innovative joining technique*. *Journal of Adhesion* (submitted).
 - [33] Boretzki, J.; Albiez, M.; Ummerhofer, T.; Myslicki, S.; Vallée, T. (2021) *Hybrid grouted joints for steel structures: experimental investigation of load-bearing and failure behaviour under static and fatigue loading*. *Journal of Constructional Steel Research* (submitted).

- [34] DIN EN 10025-1:2005 (2005) *Warmgewalzte Erzeugnisse aus Baustählen – Teil 1: Allgemeine technische Lieferbedingungen*. Berlin: Beuth.
- [35] DIN EN 196-1:2016 (2016) *Methods of testing cement – Part 1: Determination of strength*. Berlin: Beuth.
- [36] Haibach, E. (2006) *Betriebsfestigkeit: Verfahren und Daten zur Bauteilberechnung*. Berlin: Springer.
- [37] DIN EN 1993-1-9:2010 (2010) *Eurocode 3: Bemessung und Konstruktion von Stahlbauten – Teil 1-9: Ermüdung*. Berlin: Beuth.

Authors

Prof. Dr.-Ing. Thomas Ummenhofer (corresponding author)
thomas.ummenhofer@kit.edu
Karlsruhe Institute of Technology
KIT Steel and Lightweight Structures
Otto-Ammann-Platz 1
76131 Karlsruhe, Germany

Jakob Boretzki, M. Sc.
Jakob.boretzki@kit.edu
Karlsruhe Institute of Technology
KIT Steel and Lightweight Structures
Otto-Ammann-Platz 1
76131 Karlsruhe, Germany

Dr.-Ing. Matthias Albiez
matthias.albiez@kit.edu
Karlsruhe Institute of Technology
KIT Steel and Lightweight Structures
Otto-Ammann-Platz 1
76131 Karlsruhe, Germany

How to Cite this Paper

Ummenhofer, T.; Boretzki, J.; Albiez, M. (2022) *Hybrid connection technologies for hollow sections in steel construction*. Steel Construction 15, Hollow Sections, pp. 37–50.
<https://doi.org/10.1002/stco.202100048>

This paper has been peer reviewed. Submitted: 26. November 2021; accepted: 14. February 2022.